



RESEARCH ARTICLE

Adaptive fractional-order integral fast terminal sliding mode and fault-tolerant control of dual-arm robots

Le Anh Tuan¹  and Quang Phuc Ha² 

¹Vietnam Maritime University, Haiphong, Vietnam and ²Faculty of Engineering and Information Technology, University of Technology Sydney, Sydney, Australia

Corresponding author: Le Anh Tuan; Email: tuanla.ck@vimaru.edu.vn

Received: 9 September 2023; **Revised:** 22 December 2023; **Accepted:** 9 February 2024; **First published online:** 7 March 2024

Keywords: dual-arm robots; fault-tolerant control; fractional-order systems; adaptive control; sliding mode control

Abstract

Closed-loop kinematics of a dual-arm robot (DAR) often induces motion conflict. Control formulation is increasingly difficult in face of actuator failures. This article presents a new approach for fault-tolerant control of DARs based on advanced sliding mode control. A comprehensive fractional-order model is proposed taking nonlinear viscous and viscoelastic friction at the joints into account. Using integral fast terminal sliding mode control and fractional calculus, we develop two robust controllers for robots subject to motor faults, parametric uncertainties, and disturbances. Their merits rest with their strong robustness, speedy finite-time convergence, shortened reaching phase, and flexible selection of derivative orders. To avoid the need for full knowledge of faults, robot parameters, and disturbances, two versions of the proposed approach, namely adaptive integral fractional-order fast terminal sliding mode control, are developed. Here, an adaptation mechanism is equipped for estimating a common representative of individual uncertainties. Simulation and experiment are provided along with an extensive comparison with existing approaches. The results demonstrate the superiority of the proposed control technique. The robot performs well the tasks with better responses (e.g., with settling time reduced by at least 16%).

1. Introduction

Manipulators have been deployed to work in automated production lines to replace human workers to improve the productivity, quality, and consistency of outputs. Owing to the ability to mimic human behaviors, dual-arm robots are widely operated in both industrial and human-centric environments. Controlling dual-arm manipulators is an interesting topic, which can be classified into low-level control and high-level planning, wherein addressing the low-level control for DARs remains an important focus. Unlike the recent works [1–3], this paper deals with the tracking and fault-tolerant control of DARs considering nonlinear viscosity and viscoelastic friction in their joints.

In contrast to the open-loop kinematics of commonly used manipulators, DARs operate in a kinematic-closed chain. Therefore, controlling DARs is quite challenging and requires feasible techniques. Tracking control of DARs is to assure the precise motion of a gripped load according to desired paths. This issue can be rendered to the control of desired rotations of joints through the inverse kinematics.

To improve control performance, model-based control studies often enhance the robot dynamics to meet real-world requirements. Kinetic constraints in robot lead mathematical model to a form of Lagrange multipliers. A dynamic model for dual-arm mobile robots is derived in ref. [4] using recursive Gibbs-Appell formulation instead of typically using Lagrange multipliers constraints in robot lead mathematical model to a form of Lagrange multipliers. Such modeling reduced the dimension of component matrices and showed the usefulness to model-oriented control issues. Hence, if considering more features of robots and practical factors, the control formulation will be more precise and effective. In

this work, we improve the DAR dynamic model by taking nonlinear fractional frictions at joints into account. We take into account frictions at robot joints with the lubrication hybridized between wet and dry modes. This leads to a nonlinear model of damping torque characterized by two individual friction coefficients. We also consider viscoelastic friction in which damping torque is proportional to fractional derivative of displacement instead of velocity as usual. Such modeling improvements make the control formation closer to practical operation of the robots.

Together with disturbances and uncertainties, the influence of motor failures on robot operation should be adequately treated. We find the way to reduce the impact of actuator faults on the control system. Fault diagnosis and fault-tolerant control (FTC) are two typical solutions. The former focuses on fault detection while the latter tackles the control of robots in the presence of faults [5, 6]. FTC includes active and passive types. For active FTC, an observer is designed for approximating faults together with tracking goal. This method shows adaption but takes much processing time [5]. Passive FTC holds the simple structure without any fault estimation and feedback knowledge of faults [6]. It insists on keeping consistency of the output against faults without adaptive behavior. In this regard, tracking control of DARs accounting for motor faults is one of the contributions to our study.

Sliding mode control (SMC) [7–18], a robust control approach, is known to be effective in controlling manipulators. While possessing strong robustness against uncertainties and disturbances, SMC is, on the other hand, subject to some drawbacks, for instance, highly switching gains, long convergence time, and chattering in the response. Fortunately, there have been some techniques dealing with these issues. Along with tracking and maintaining the system robustness, optimal SMC minimizes the energy of control inputs using the state-dependent Riccati technique [7]. Terminal sliding mode control (TSMC) [8] and fast terminal sliding mode (FTSMC) [10] can achieve rapid finite-time stabilization. High-order SMC [10, 11] reduces the output chattering but takes much time for convergence. Similar to the goal of super-twisting SMC [12], logarithmic SMC introduces logarithm function in terms of states into control structure to reduce chattering of control signals [12]. Specifically, integral TSMC [13] is effective in alleviating chattering and improving further steady-state performance. Therefore, combining integral action into FTSMC is one of the feasible choices for controlling DARs.

While SMC-based algorithms [7–18] can maintain well the tracking performance, they lack the ability to adjust control parameters in response to large system uncertainties. As a remedy, adaptive control approaches have been integrated into the SMC. Along with traditional adaptation approaches such as model-reference adaptive control and self-tuning control (STC) [19], the modern adaptive trends have been recently developed and rapidly applied for DARs [20–23]. Advances in computer science have significantly contributed to intelligent control of DARs [22–25]. Different types of machine learning have been applied to many areas including robotics. Machine learning-based techniques, such as neural control [20, 21], composite learning [22], and brain-actuated control [23], have been successfully applied for DARs. Although learning often involves complex computation and increases the processing time, it offers a promising solution to manipulator control. As such, DARs can learn to detect errors and conduct advanced tasks in unstructured environments intelligently, precisely, and robustly. In ref. [22], learning algorithms are combined with online neural networks for supporting the DAR controllers. Using the human-inspired approach and human-robot interactions, bimanual controllers are developed based on various techniques such as humanoid stiffness identification [24] and impedance control [25]. To this end, human skills can effectively transfer to DARs for both control and motion planning objectives, for example, online brain-machine interface and support vector machines have been used to design a bimanual controller for DARs [26]. Indeed, with artificial intelligence-based techniques [20–25], the modern DARs nowadays are approaching closer to human responses.

The development of fractional calculus provides an effective mathematical tool for enhancing control performance [26]. Therein, the control algorithms contain fractional derivatives with adjustable orders. In reality, fractional-order control (FOC) is not a single technique, but rather is combined with a primary control core. FOC-integrated SMC was successfully applied to various plants such as single-arm robots [16, 17, 27] and knee joint [28]. Recently, FOC was also combined with SMC for dual-arm robots [29] in which their adaptive feature is accompanied by a neural networks-based estimator. While DARs are

fully actuated systems [29], we enhanced an adaptive fractional-order SMC approach to under-actuated systems, such as a tower crane [30].

The above review indicates that various control approaches may be attributed to different advantages and weaknesses. We thus access a suitable control formulation of DARs by utilizing their control merits while overcoming drawbacks. Motivated by the recent works [29, 30] on adaptive fractional-order SMC-based control approaches, our aim is to develop a control system that can amalgamate the merits of integral control, FOC, FTC, and adaptive STC. Indeed, the proposed I-FTSMC core can achieve strong robustness, time-reduction at the reaching phase, and quick finite-time convergence. Fractional derivatives in the control structure play an important role in control parameter fine-tuning to obtain the best performance. An adaptation observer, set on the feedback loop, can estimate the impact simultaneously of faults of motors, uncertain robot parameters, and unknown disturbances. Such combination, applied to DARs, results in the key contributions in terms of modeling and control:

- a. For modeling, a comprehensive model for DAR dynamics is obtained as a fractional-order system considering not only nonlinear viscoelasticity of joints, parametric uncertainties, and system disturbances but also faults of actuators.
- b. For control development, a new control system integrating advantages of I-FTSMC, FTC, FOC, and adaptive techniques. They feature robustness as well as rapid finite-time stability and chattering reduction by I-FTSMC, flexibility in the control structure with FOC, and adaptation by FTC combined with STC for concurrently estimating robot parameters, disturbances, and faults of actuators.

As a result, the proposed control system achieves strong robustness, high adaptation, and resilience in terms of responding to uncertainties via its self-learning capability. In comparison to ref. [30], the difference of this work lies in key facts: (i) fractional-order differential equations describe robot dynamics instead of ordinary differential equations as seen in ref. [30], (ii) A DAR is a fully-actuated system holding closed-loop kinetic chain while under-actuated systems in ref. [30], such as tower cranes, hold open kinetic constraint, (iii) Unlike [30] utilizing linear sliding surface, the current study applies an integral sliding mode for lightening the chattering phenomenon, and (iv) The 2nd scheme of FTSMC controller in this study is an enhancement of the control core described in ref. [30]. Generally, our adaptive robust controller for DARs displays the following new features:

1. Unlike the controllers [20–23] containing fixed integer orders of derivatives, here variable fractional derivatives are used for control. By considering fractional orders as flexible control parameters, we can tune them to achieve the optimal robot performance.
2. While adaptive approaches using neural networks [20, 21, 29], machine learning [22–25], and fuzzy logic [31, 32] often encounter a complex configuration and computational latency, our three-in-one adaptation mechanism shows effectiveness in estimation and processing capability. Indeed, the multifunctional mechanism of our development identifies equivalently a unified component for approximating faults, uncertain parameters, and unknown disturbances.

The article is organized as follows. Section 2 introduces the preliminaries for control design. Section 3 presents a fractional-order dynamic model for DARs taking into account nonlinear viscoelastic lubrication of joints, faults of motors, parametric variations, and unknown disturbances. Using FTC-combined I-FTSMC, two robust controllers are developed in Section 4, based on Mittag-Leffler stability. In Section 5, adaptive features are augmented to the robust controllers via the synthesis of adaptation mechanism to approximate unknowns and uncertainties. Section 6 provides results to demonstrate effectiveness of the proposed approach in simulation and experiments with a laboratorial DAR. Comparative analysis with various control approaches is also included. Finally, a conclusion and future work are discussed in Section 7.

2. Preliminaries

Some preliminaries on fractional-order systems and terminal stability are briefly reviewed in this section. In this study, we thoroughly apply Caputo definition for fractional derivatives in the analytical analysis, numerical simulation, and experiment. From now on, $D_t^\alpha(\bullet)$ indicates Caputo's derivative of (\bullet) with fractional order α with respect to time t .

Definition 1 [33]: We consider a fractional-order system

$$D_t^\alpha \mathbf{x}(t) = f(\mathbf{x}(t)), \tag{1}$$

where $\alpha \in (0, 1)$, $\mathbf{x}(t) \in \mathbb{R}^n$. The solution $\mathbf{x}(t)$ of (1) is said to be Mittag-Leffler stable if

$$\|\mathbf{x}(t)\| \leq \{m[\mathbf{x}(t_0)]E_\alpha(-\lambda(t-t_0)^\alpha)\}^b, \tag{2}$$

where t_0 is the initial time, $\lambda > 0$, $b > 0$, $m(\mathbf{0}) = 0$, $m(\mathbf{x}) \geq \mathbf{0}$, $m(\mathbf{x})$ is locally Lipschitz on $\mathbf{x} \in \mathbb{R}^n$, and $E_\alpha(\bullet)$ is the Mittag-Leffler function defined by

$$E_\alpha(z) = \sum_{k=0}^{\infty} \frac{z^k}{\Gamma(k\alpha + 1)} \tag{3}$$

Now recall that a function $\kappa_i(t)$ is of the so-called class kappa if it is continuously increasing and $\kappa_i(0) = 0$. In the following lemma, positive definite functions κ_i ($i = 1-3$) are class kappa functions [34].

Lemma 1 [33]: If there exists for the system (1) a Lyapunov function $V(\mathbf{x}, t)$ continuously differentiable satisfying

$$\kappa_1 \|\mathbf{x}\| \leq V(\mathbf{x}, t) \leq \kappa_2 \|\mathbf{x}\| \tag{4}$$

and

$$D_t^\alpha V(\mathbf{x}, t) \leq -\kappa_3 \|\mathbf{x}\| \tag{5}$$

with $\alpha \in (0, 1)$ and $\kappa_1, \kappa_2, \kappa_3$ being class kappa functions, then system (1) is Mittag-Leffler stable with equilibrium $\mathbf{x} = \mathbf{0}$.

Notably, Mittag-Leffer stability implies asymptotic stability. When $\alpha = 1$, Mittag-Leffler function (3) can reduce to an exponential function, and in that case Mittag-Leffer stability is also exponential stability.

Lemma 2 [35]: Let $\mathbf{x}(t) \in \mathbb{R}^n$ be a vector of continuously differentiable real functions. For all time instant $t \geq t_0$, the following inequality holds:

$$D_t^\alpha \left(\frac{1}{2} \mathbf{x}^T(t) \mathbf{Q} \mathbf{x}(t) \right) \leq \mathbf{x}^T(t) \mathbf{Q} D_t^\alpha \mathbf{x}(t), \tag{6}$$

for any fractional order $\alpha \in (0, 1)$, in which $\mathbf{Q} \in \mathbb{R}^{n \times n}$ is a positive-definite matrix.

Consider fractional-order system (1) with state vector $\mathbf{x}(t)$ satisfying (6). By applying Lemma 1 to a Lyapunov function

$$V(\mathbf{x}(t)) = \frac{1}{2} \mathbf{x}^T(t) \mathbf{x}(t), \tag{7}$$

and $\mathbf{Q} = \mathbf{1}$, one obtains the following corollary.

Corollary 1 [36]: If the following condition holds

$$\mathbf{x}^T(t) f(\mathbf{x}(t)) \leq 0, \tag{8}$$

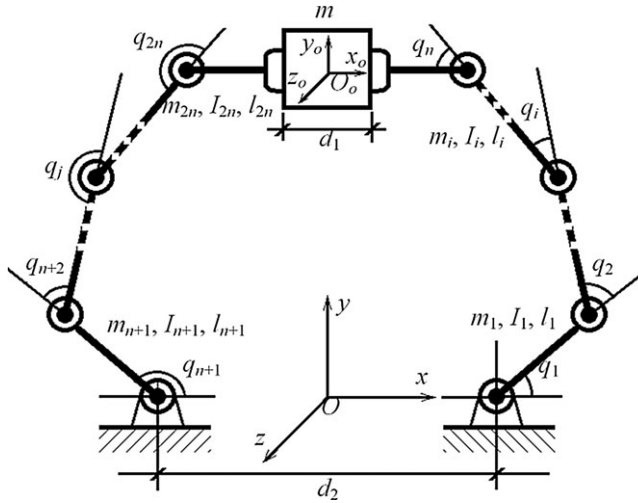


Figure 1. 2n-DOF modeling of a dual-arm robot.

then the origin $\mathbf{x} = \mathbf{0}$ of system (1) is stable. And if

$$\mathbf{x}^T(t)f(\mathbf{x}(t)) < 0, \tag{9}$$

then the system (1) is asymptotically stable to the equilibrium $\mathbf{x} = \mathbf{0}$.

Lemma 3 [37]: If there exists a continuously differentiable positive function $V(\mathbf{x})$ with $\mathbf{x}(t) \in \mathbb{R}^n$ of system (1) such that

$$\dot{V}(\mathbf{x}) \leq -\chi V(\mathbf{x}) - \delta V^\vartheta(\mathbf{x}) \forall t > t_0 \tag{10}$$

for each gain $0 \leq \vartheta \leq 1$, $\chi > 0$, and $\delta > 0$, then $V(\mathbf{x})$ is asymptotically convergent with a terminal time

$$t_s \leq \frac{1}{\chi(1-\vartheta)} \ln \frac{\chi V^{1-\vartheta}(\mathbf{x}(0)) + \delta}{\delta}. \tag{11}$$

3. Enhanced modeling of dual-arm robots

A conventional model of DARs was represented in ref. [20]. In this paper, we seek a dynamic model for DARs that can also incorporate practical factors during the robot’s operation. They include (i) non-linear damping and fractional frictions at joints, (ii) faults of motors, and (iii) uncertain parameters and unknown disturbances.

Consider the diagram shown in Fig. 1 for a DAR picking up and moving an object m to a destination. Each arm has r links including its end-effector and n rotating angles at joints. Each link is considered a rigid body characterized by four physical parameters composed of mass m_i , length l_i , rotational inertia I_i , and distance k_i from joint to the mass center. Therein, a DAR has $2r$ links and $2n$ generalized coordinates $\mathbf{q} \in \mathbb{R}^{2n}$ in which $2n$ servo motors having torques $\mathbf{T} \in \mathbb{R}^{2n}$ as control inputs. The DAR dynamics is described as

$$\mathbf{M}(\mathbf{q})\ddot{\mathbf{q}} + \mathbf{C}(\mathbf{q}, \dot{\mathbf{q}})\dot{\mathbf{q}} + \hat{\mathbf{B}}(\boldsymbol{\mu}, D_i^n \mathbf{q}, \hat{\mathbf{b}})D_i^n \mathbf{q} + \mathbf{G}(\mathbf{q}) = \mathbf{J}^T(\mathbf{q})\hat{\mathbf{F}}(\mathbf{q}, \dot{\mathbf{q}}, \ddot{\mathbf{q}}, \hat{m}) + \boldsymbol{\eta}^T(t - T_f)\boldsymbol{\phi}(\dot{\mathbf{q}}, \mathbf{q}, \mathbf{T}) + \mathbf{T} + \hat{\mathbf{D}}, \tag{12}$$

where $\mathbf{M}(\mathbf{q}) = \mathbf{M}^T(\mathbf{q}) \in \mathbb{R}^{2n \times 2n}$ denotes a positive-definite matrix of inertia, $\mathbf{C}(\mathbf{q}, \dot{\mathbf{q}}) \in \mathbb{R}^{2n \times 2n}$ indicates a centripetal Coriolis matrix, $\mathbf{G}(\mathbf{q}) \in \mathbb{R}^{2n}$ represents the gravitational torque, $\mathbf{J}(\mathbf{q}) \in \mathbb{R}^{2n \times 2n}$ is a Jacobian matrix, $\hat{\mathbf{B}}(\boldsymbol{\mu}, D_i^n \mathbf{q}, \hat{\mathbf{b}})$ is a viscoelastic damping matrix, $\hat{\mathbf{F}}(\mathbf{q}, \dot{\mathbf{q}}, \ddot{\mathbf{q}}, \hat{m})$ is a vector of reaction forces between

load and two end-effectors, and $\hat{\mathbf{D}} \in \mathbb{R}^{2n}$ is a vector of unknown disturbances. In comparison with the model presented in ref. [20], dynamics (12) extends the model to include the following considerations:

3.1. Nonlinear viscous and fractional friction at joints

The term $\hat{\mathbf{B}}(\boldsymbol{\mu}, D_i^\eta \mathbf{q}, \hat{\mathbf{b}})D_i^\eta \mathbf{q}$ in dynamics (12) shows nonlinear viscosity and fractional friction at the robot’s joints. Normally, it is $\mathbf{B}\dot{\mathbf{q}}$ for linear viscous at joints. In many cases, the lubrication at joints corresponds to adequate Reynolds in which the wet friction lies between linear and quadratic forms, that is

$$T_i^f = c_i |\dot{q}_i|^{\mu_i} \dot{q}_i, \tag{13}$$

where $0 < \mu_i < 1$ and c_i ($i = 1-2n$) are viscous coefficients. Additionally, viscoelasticity of lubricating oil leads to a fractional-derivative model of friction at joints

$$T_i^f = b_i D_i^{\eta_i} q_i, \tag{14}$$

where $\eta_i \in (0,1)$ is the fractional order of the derivative and b_i is a viscoelasticity coefficient. Combination of nonlinear viscosity (13) with fractional friction (14) leads to a nonlinear fractional-order model

$$T_i^f = b_i |D_i^{\eta_i} q_i|^{\mu_i} D_i^{\eta_i} q_i, \tag{15}$$

which is represented comprehensively by the term $\hat{\mathbf{B}}(\boldsymbol{\mu}, D_i^\eta \mathbf{q}, \hat{\mathbf{b}})D_i^\eta \mathbf{q}$ of Eq. (12). Here, for a $2n$ -DOF model, $\hat{\mathbf{B}}(\boldsymbol{\mu}, D_i^\eta \mathbf{q}, \hat{\mathbf{b}}) = \text{diag}(\hat{b}_i |D_i^\eta q_i|^{\mu_i}) \in \mathbb{R}^{2n \times 2n}$ with $\boldsymbol{\mu} = [\mu_i]^T \in \mathbb{R}^{2n}$, $0 < \eta < 1$, and $0 < \mu_i < 1$. Moreover, the component $\mathbf{C}(\mathbf{q}, \dot{\mathbf{q}}) + \hat{\mathbf{B}}(\boldsymbol{\mu}, D_i^\eta \mathbf{q}, \hat{\mathbf{b}})$ is a skew symmetric matrix satisfying $\mathbf{q}^T \{\dot{\mathbf{M}}(\mathbf{q}) - 2[\mathbf{C}(\mathbf{q}, \dot{\mathbf{q}}) + \hat{\mathbf{B}}(\boldsymbol{\mu}, D_i^\eta \mathbf{q}, \hat{\mathbf{b}})]\} \mathbf{q} = 0 \forall \mathbf{q} \in \mathbb{R}^{2n}$.

3.2. Faults of motors

The term $\boldsymbol{\eta}^T(t - t_f)\boldsymbol{\phi}(\dot{\mathbf{q}}, \mathbf{q}, \mathbf{T})$ in robot dynamics (12) represents the influence of actuator faults. Here, $\boldsymbol{\phi}(\dot{\mathbf{q}}, \mathbf{q}, \mathbf{T}) \in \mathbb{R}^{2n}$ is the fault function [6] characterized by faulty components taking place the system. The term $\boldsymbol{\eta}(t - t_f) = \text{diag}[\eta_i(t - t_f)] \in \mathbb{R}^{m \times m}$ denotes the temporal profile of faults described as

$$\eta_i(t - t_f) = \begin{cases} 0 & \text{if } t < t_f \\ 1 - \exp[-a_i(t - t_f)] & \text{if } t \geq t_f \end{cases} \tag{16}$$

where a_i is the evolution rate of an unknown fault. Here, a fault is considered as incipient or abrupt respectively for small or big values of a_i , t_f indicates the time of fault occurrence, and η_i represents the fault effects.

3.3. Unknown disturbances and parametric uncertainties

Unknown perturbances are described by adjustable term $\hat{\mathbf{D}}$ in model (12) that will be estimated by an adaptive mechanism. Uncertainties always exist in the system, e.g., mass m may change up to each operation case, or joint frictions b_i may vary depending on working environment and lubrication. Taking this into account, we introduce vector $\hat{\mathbf{p}} = \text{diag}(\hat{m}, \hat{\mathbf{b}}) \in \mathbb{R}^{2n+1}$ with $\hat{\mathbf{b}} = \text{diag}(\hat{b}_i) \in \mathbb{R}^{2n}$. Correspondingly, matrix $\hat{\mathbf{B}}(\boldsymbol{\mu}, D_i^\eta \mathbf{q}, \hat{\mathbf{b}})$ and vector $\hat{\mathbf{F}}(\mathbf{q}, \dot{\mathbf{q}}, \ddot{\mathbf{q}}, \hat{m})$ in Eq. (12) can be parameterized in terms of $\hat{\mathbf{b}}$ and \hat{m} . Robot model (12) is then rewritten as

$$\mathbf{M}(\mathbf{q})\ddot{\mathbf{q}} + \mathbf{C}(\mathbf{q}, \dot{\mathbf{q}})\dot{\mathbf{q}} + \mathbf{G}(\mathbf{q}) = \mathbf{T} + \mathbf{U}(\mathbf{q}, \dot{\mathbf{q}}, \ddot{\mathbf{q}}, \hat{\mathbf{p}}, \boldsymbol{\phi}, \hat{\mathbf{D}}), \tag{17}$$

where the complex term

$$\mathbf{U}(\mathbf{q}, \dot{\mathbf{q}}, \ddot{\mathbf{q}}, \hat{\mathbf{p}}, \boldsymbol{\phi}, \hat{\mathbf{D}}) = \overline{\mathbf{U}}(\mathbf{q}, \dot{\mathbf{q}}, \ddot{\mathbf{q}}, \hat{\mathbf{p}}, \boldsymbol{\phi}) + \hat{\mathbf{D}}, \tag{18}$$

in which

$$\overline{\mathbf{U}}(\mathbf{q}, \dot{\mathbf{q}}, \ddot{\mathbf{q}}, \hat{\mathbf{p}}, \boldsymbol{\phi}) = \boldsymbol{\eta}^T(t - T_f)\boldsymbol{\phi}(\dot{\mathbf{q}}, \mathbf{q}, \mathbf{T}) - \hat{\mathbf{B}}(\boldsymbol{\mu}, D_i^\eta \mathbf{q}, \hat{\mathbf{b}})D_i^\eta \mathbf{q} + \mathbf{J}^T(\mathbf{q})\hat{\mathbf{F}}(\mathbf{q}, \dot{\mathbf{q}}, \ddot{\mathbf{q}}, \hat{m}), \tag{19}$$

Table I. Two phases of convergence.

	Scheme 1	Scheme 2
Phase 1	Terminal sliding manifold $\dot{\mathbf{s}} + \boldsymbol{\beta}\mathbf{s} + \boldsymbol{\lambda}\mathbf{s}^{\zeta_1} + \mathbf{K} \operatorname{sgn}(\mathbf{s}) = \mathbf{0}$	Sliding manifold $\dot{\mathbf{s}} + \boldsymbol{\beta}\mathbf{s} + \mathbf{K} \operatorname{sgn}(\mathbf{s}) = \mathbf{0}$
Phase 2	Asymptotic convergence of outputs $D_t^\alpha \mathbf{e} + \boldsymbol{\beta}\mathbf{e} = \mathbf{0}$	Terminal convergence of outputs $D_t^\alpha \mathbf{e} + \boldsymbol{\beta}\mathbf{e} + \boldsymbol{\gamma}\mathbf{e}^{\zeta_2} = \mathbf{0}$

containing information of faults $\boldsymbol{\phi}$ and uncertain parameters $\hat{\mathbf{p}}$ is bounded by

$$\|\bar{\mathbf{U}}(\mathbf{q}, \dot{\mathbf{q}}, \ddot{\mathbf{q}}, \hat{\mathbf{p}}, \boldsymbol{\phi})\| < U_1 + U_2\|\mathbf{q}\| + \dots + U_{2n}\|\mathbf{q}\|^{2n-1}. \tag{20}$$

Here, U_1, U_2, \dots, U_{2n} are positive constants. Given that disturbances $\hat{\mathbf{D}}$ is a bounded function, condition (20) implies that $\mathbf{U}(\mathbf{q}, \dot{\mathbf{q}}, \ddot{\mathbf{q}}, \hat{\mathbf{p}}, \boldsymbol{\phi}, \hat{\mathbf{D}})$ (18) is bounded. Since $\mathbf{M}(\mathbf{q})$ is positive definite, Eq. (17) can now be rewritten as

$$\ddot{\mathbf{q}} = \mathbf{M}^{-1}(\mathbf{q})[T + \mathbf{U}(\mathbf{q}, \dot{\mathbf{q}}, \ddot{\mathbf{q}}, \hat{\mathbf{p}}, \hat{\mathbf{D}}, \boldsymbol{\phi}) - \mathbf{C}(\mathbf{q}, \dot{\mathbf{q}})\dot{\mathbf{q}} - \mathbf{G}(\mathbf{q})]. \tag{21}$$

Remark 1: Dynamic model (21) or (18) is effective for constructing an adaptive robust controller. With the integration of adaptation mechanism, the controller only needs to estimate the equivalence $\mathbf{U}(\mathbf{q}, \dot{\mathbf{q}}, \ddot{\mathbf{q}}, \hat{\mathbf{p}}, \boldsymbol{\phi}, \hat{\mathbf{D}})$ instead of identifying faults $\boldsymbol{\phi}$, uncertain parameters $\hat{\mathbf{p}}$, and unknown disturbance $\hat{\mathbf{D}}$, separately.

Remark 2: The kinematics of DARs show the relationship between an object path and rotations of links, from which motion equations of object are obtained [20]. Based on motion path $\mathbf{r}(x, y, z, t)$ of object m , the joint angles $\mathbf{q}(t)$ can be derived by using inverse kinematics. Thus, tracking control of a DAR according to reference trajectory $\mathbf{r}_d(x, y, z, t)$ of the object is equivalent to tracking joint rotations $\mathbf{q}(t)$ to their destinations $\mathbf{q}_d(t)$.

4. Integral fractional-order fast terminal sliding mode control

We propose two control schemes for tracking vector $\mathbf{q}(t)$ of robot joints to its destinations $\mathbf{q}_d(t)$. Control structures contain then fractional derivative, finite integral, and terminal convergence terms. Tracking the outputs includes two phases: the convergence to the sliding surface in the first phase and driving the outputs to destinations at the second phase. These control laws hold the distinct ways of convergence that are summarized in Table I.

We begin with scheme 1 by the following theorem:

Theorem 1: Control scheme

$$\mathbf{T} = \mathbf{M}(\mathbf{q})\{\ddot{\mathbf{q}}_d - D_t^{2-\alpha}[\boldsymbol{\beta}(\mathbf{e} + \mathbf{s}) + \boldsymbol{\lambda}\mathbf{s}^{\zeta_1} + \mathbf{K} \operatorname{sgn}(\mathbf{s})]\} + \mathbf{C}(\mathbf{q}, \dot{\mathbf{q}})\dot{\mathbf{q}} + \mathbf{G}(\mathbf{q}) - \mathbf{U}(\mathbf{q}, \dot{\mathbf{q}}, \ddot{\mathbf{q}}, \mathbf{p}, \mathbf{D}, \boldsymbol{\phi}) \tag{22}$$

with sliding function

$$\mathbf{s} = \int_0^t (D_t^\alpha \mathbf{e} + \boldsymbol{\beta}\mathbf{e})dt, \tag{23}$$

asymptotically drives the robot outputs $\mathbf{q}(t)$ governed by dynamics (17 and 18) to references $\mathbf{q}_d(t)$. Here, $\mathbf{e} = (\mathbf{q} - \mathbf{q}_d) \in \mathbb{R}^{2n}$ is the tracking error and function $\mathbf{s}(t) \in \mathbb{R}^{2n}$ contains a fractional derivative D_t^α with $\alpha \in (0, 1)$; $\operatorname{sgn}(\bullet)$ is a signum function; control gains $\boldsymbol{\beta} = \operatorname{diag}(\beta_1, \dots, \beta_{2n})$, $\boldsymbol{\lambda} = \operatorname{diag}(\lambda_1, \dots, \lambda_{2n})$, $\mathbf{K} = \operatorname{diag}(K_1, \dots, K_{2n})$ are positive-definite matrices; and terminal gain ζ_1 is bounded by $-1 \leq \zeta_1 \leq 1$.

Proof: Consider the positive Lyapunov function

$$V = \frac{1}{2} \mathbf{s}^T \mathbf{s} = \frac{1}{2} \sum_{i=1}^{2n} s_i^2 \tag{24}$$

whose time derivative is

$$\dot{V} = \mathbf{s}^T \dot{\mathbf{s}} = \sum_{i=1}^{2n} s_i \dot{s}_i. \tag{25}$$

Derivative of function (23) with respect to time is given by

$$\dot{\mathbf{s}} = D_t^{\alpha-2}(\ddot{\mathbf{q}} - \ddot{\mathbf{q}}_d) + \boldsymbol{\beta}(\mathbf{q} - \mathbf{q}_d), \tag{26}$$

that leads the Lyapunov derivative (25) to

$$\dot{V} = \mathbf{s}^T [D_t^{\alpha-2}(\ddot{\mathbf{q}} - \ddot{\mathbf{q}}_d) + \boldsymbol{\beta}(\mathbf{q} - \mathbf{q}_d)]. \tag{27}$$

Inserting robot dynamics (21) into (27) results in

$$\dot{V} = \mathbf{s}^T \{D_t^{\alpha-2}[\mathbf{M}^{-1}(\mathbf{T} + \mathbf{U} - \mathbf{C}\dot{\mathbf{q}} - \mathbf{G}) - \ddot{\mathbf{q}}_d] + \boldsymbol{\beta}(\mathbf{q} - \mathbf{q}_d)\}. \tag{28}$$

Applying control scheme (22) to Lyapunov derivative (28) yields

$$\dot{V} = -\mathbf{s}^T \boldsymbol{\beta} \mathbf{s} - \mathbf{s}^T \boldsymbol{\lambda} \mathbf{s}^{\zeta_1} - \mathbf{s}^T \mathbf{K} \operatorname{sgn}(\mathbf{s}) \tag{29}$$

which leads to

$$\begin{aligned} \dot{V} &= -\sum_{i=1}^{2n} \beta_i s_i^2 - \sum_{i=1}^{2n} \lambda_i s_i^{\zeta_1+1} - \sum_{i=1}^{2n} K_i |s_i| \\ &\leq -\beta_{\min} \sum_{i=1}^{2n} s_i^2 - \lambda_{\min} \sum_{i=1}^{2n} s_i^{\zeta_1+1} - \sum_{i=1}^{2n} K_i |s_i| \\ &= -2\beta_{\min} V(\mathbf{x}) - 2\lambda_{\min} V(\mathbf{x})^{\frac{\zeta_1+1}{2}} - \sum_{i=1}^{2n} K_i |s_i| \\ &\leq -2\beta_{\min} V(\mathbf{x}) - 2\lambda_{\min} V(\mathbf{x})^{\frac{\zeta_1+1}{2}} \end{aligned} \tag{30}$$

where $\beta_{\min} = \min(\beta_1, \dots, \beta_{2n})$ and $\lambda_{\min} = \min(\lambda_1, \dots, \lambda_{2n})$. Applying the Lemma 3 for $\chi = 2\beta_{\min}$, $\delta = 2\lambda_{\min}$, and $2\vartheta = \zeta_1 + 1$, one concludes that the sliding function asymptotically converges to zero with the reaching finite-time bounded by

$$t_s = \frac{1}{\beta_{\min}(1 - \zeta_1)} \ln \frac{2\beta_{\min} V^{\frac{1-\zeta_1}{2}}(\mathbf{x}(t_o)) + 2\lambda_{\min}}{2\lambda_{\min}}. \tag{31}$$

Zero convergence of sliding function (28) means

$$D_t^\alpha(\mathbf{q} - \mathbf{q}_d) + \boldsymbol{\beta}(\mathbf{q} - \mathbf{q}_d) = \mathbf{0}, \tag{32}$$

or equivalently,

$$D_t^\alpha \mathbf{e}(t) = f(\mathbf{e}(t)) = -\boldsymbol{\beta} \mathbf{e}(t). \tag{33}$$

By applying Corollary 1 for $\mathbf{x}(t) = \mathbf{e}(t)$, one can obtain

$$\mathbf{e}(t)^T f(\mathbf{e}(t)) = -\mathbf{e}(t)^T \boldsymbol{\beta} \mathbf{e}(t) \leq 0 \tag{34}$$

for every $\mathbf{e}(t) \in \mathbb{R}^{2n}$ and diagonal matrix $\boldsymbol{\beta} = \operatorname{diag}(\beta_i) \in \mathbb{R}^{2n \times 2n}$ of gains $\beta_i > 0$. Therefore, Corollary 1 indicates that the tracking error $\mathbf{e}(t)$ is Mittag-Leffler stable with a convergence form

$$\mathbf{e}(t) = \mathbf{e}(t) E_\alpha(\boldsymbol{\beta} t^\alpha), \tag{35}$$

In other words, $\mathbf{q}(t)$ asymptotically approaches to $\mathbf{q}_d(t)$.

We propose scheme 2 through the following theorem:

Theorem 2: Control scheme

$$\mathbf{T} = \mathbf{M}(\mathbf{q})\{\ddot{\mathbf{q}}_d - D_t^{2-\alpha}[\boldsymbol{\beta}\mathbf{e} + \boldsymbol{\gamma}\mathbf{e}^{\zeta_2} + \boldsymbol{\beta}\mathbf{s} + \mathbf{K} \operatorname{sgn}(\mathbf{s})]\} + \mathbf{C}(\mathbf{q}, \dot{\mathbf{q}})\dot{\mathbf{q}} + \mathbf{G}(\mathbf{q}) - \mathbf{U}(\mathbf{q}, \dot{\mathbf{q}}, \ddot{\mathbf{q}}, \mathbf{p}, \mathbf{D}, \boldsymbol{\Phi}) \quad (36)$$

with the terminal sliding function

$$\mathbf{s} = \int_0^t (D_t^\alpha \mathbf{e} + \boldsymbol{\beta}\mathbf{e} + \boldsymbol{\gamma}\mathbf{e}^{\zeta_2})dt, \quad (37)$$

asymptotically drives the robot outputs $\mathbf{q}(t)$ to references $\mathbf{q}_d(t)$ in finite time. Here, $\boldsymbol{\gamma} = \operatorname{diag}(\gamma_1, \dots, \gamma_{2n})$ is a positive-definite matrix of control gains, and ζ_2 is an odd integer.

Proof: Again, we choose the positive Lyapunov candidate

$$V = \frac{1}{2}\mathbf{s}^T\mathbf{s} = \frac{1}{2} \sum_{i=1}^{2n} s_i^2 \quad (38)$$

with time derivative

$$\dot{V} = \mathbf{s}^T\dot{\mathbf{s}} = \sum_{i=1}^{2n} s_i\dot{s}_i. \quad (39)$$

Differentiating (37) with respect to time result in

$$\dot{\mathbf{s}} = D_t^{\alpha-2}\ddot{\mathbf{e}} + \boldsymbol{\beta}\mathbf{e} + \boldsymbol{\gamma}\mathbf{e}^{\zeta_2} \quad (40)$$

that leads Lyapunov derivative (39) to

$$\dot{V} = \mathbf{s}^T(D_t^{\alpha-2}\ddot{\mathbf{e}} + \boldsymbol{\beta}\mathbf{e} + \boldsymbol{\gamma}\mathbf{e}^{\zeta_2}). \quad (41)$$

Respectively substituting robot dynamics (21) and control law (36) into Eq. (41) yields

$$\dot{V} = \mathbf{s}^T\{D_t^{\alpha-2}[\mathbf{M}^{-1}(\mathbf{T} + \mathbf{U} - \mathbf{C}\dot{\mathbf{q}} - \mathbf{G}) - \ddot{\mathbf{q}}_d] + \boldsymbol{\beta}\mathbf{e} + \boldsymbol{\gamma}\mathbf{e}^{\zeta_2}\}, \quad (42)$$

which can be reduced to

$$\dot{V} = -\mathbf{s}^T\boldsymbol{\beta}\mathbf{s} - \mathbf{s}^T\mathbf{K} \operatorname{sgn}(\mathbf{s}) = - \sum_{i=1}^{2n} \beta_i s_i^2 - \sum_{i=1}^{2n} K_i |s_i| \leq 0 \quad (43)$$

for all $\beta_i > 0$ and $K_i > 0$. This implies that $V(t) \leq V(0)$ or \mathbf{s} is bounded. Alternatively, the second derivative of Lyapunov function (38) is

$$\ddot{V} = - \left\{ \dot{\mathbf{s}}^T\boldsymbol{\beta}\mathbf{s} + \mathbf{s}^T\boldsymbol{\beta}\dot{\mathbf{s}} + \mathbf{s}^T\mathbf{K} \left[\frac{d \operatorname{sgn}(s_i)}{ds_i} \dot{s}_i \right]_{2n \times 1} + \dot{\mathbf{s}}^T\mathbf{K} \operatorname{sgn}(\mathbf{s}) \right\} \quad (44)$$

Notably, derivative of the signum function is equal to zero except at zero. Hence,

$$\ddot{V} = -[\dot{\mathbf{s}}^T\boldsymbol{\beta}\mathbf{s} + \mathbf{s}^T\boldsymbol{\beta}\dot{\mathbf{s}} + \dot{\mathbf{s}}^T\mathbf{K} \operatorname{sgn}(\mathbf{s})] \quad \forall \mathbf{s} \neq \mathbf{0} \quad (45)$$

We substitute reduced-order dynamics (21) and control inputs (36) into manifold derivative (40), then we get

$$\dot{\mathbf{s}} = -\boldsymbol{\beta}\mathbf{s} - \mathbf{K} \operatorname{sgn}(\mathbf{s}) \quad (46)$$

Eq. (46) shows that $\dot{\mathbf{s}}$ is bounded because \mathbf{s} is a bounded vector and \mathbf{K} and $\boldsymbol{\beta}$ are positive-definite matrices. Therefore, \ddot{V} (45) is bounded and thus \dot{V} is uniformly continuous in time. Application of Barbalat’s lemma yields $\lim_{t \rightarrow \infty} \dot{V} = 0$, which $\lim_{t \rightarrow \infty} s = 0$. Hence, the manifold (37) is asymptotically stable that results in

$$D_t^\alpha \mathbf{e} = -\boldsymbol{\beta}\mathbf{e} - \boldsymbol{\gamma}\mathbf{e}^{\zeta_2}, \quad (47)$$

We analyze the stability of dynamics (47) with a Lyapunov function

$$V = 0.5(\mathbf{e}^T\mathbf{e} + \mathbf{s}^T\mathbf{s}) > 0. \quad (48)$$

By applying Lemma 2, fractional derivative of Lyapunov (48) satisfies

$$D_t^\alpha V = D_t^\alpha 0.5(\mathbf{e}^T \mathbf{e} + \mathbf{s}^T \mathbf{s}) \leq \mathbf{e}^T D_t^\alpha \mathbf{e} + \mathbf{s}^T D_t^\alpha \mathbf{s}. \tag{49}$$

Combining Eq. (47), fractional derivative, $D_t^\alpha \mathbf{s} = D_t^{\alpha-1}(D_t^\alpha \mathbf{e} + \beta \mathbf{e} + \gamma \mathbf{e}^{\zeta_2})$, of manifold (37), robot dynamics (21), and controller (36) with inequality (49) leads to

$$D_t^\alpha V \leq -\mathbf{e}^T (\beta \mathbf{e} + \gamma \mathbf{e}^{\zeta_2}) + \mathbf{s}^T D_t^{\alpha-1}(D_t^\alpha \mathbf{e} + \beta \mathbf{e} + \gamma \mathbf{e}^{\zeta_2}) = -\mathbf{e}^T \beta \mathbf{e} - \mathbf{e}^T \gamma \mathbf{e}^{\zeta_2} - \mathbf{s}^T \beta D_t^{\alpha-1} \mathbf{s} - \mathbf{s}^T \mathbf{K} D_t^{\alpha-1} \text{sgn}(\mathbf{s}) \tag{50}$$

Once \mathbf{s} approach zeros, inequality (50) becomes

$$D_t^\alpha V \simeq -\mathbf{e}^T \beta \mathbf{e} - \mathbf{e}^T \gamma \mathbf{e}^{\zeta_2} = -\sum_{i=1}^{2n} \beta_i e_i^2 - \sum_{i=1}^{2n} \gamma_i e_i^{\zeta_2+1} \leq -\sum_{i=1}^{2n} \beta_i e_i^2 \leq -\kappa_3 \|\mathbf{e}\| \tag{51}$$

$\forall \beta_i > 0, \gamma_i > 0$, where κ_3 is an arbitrary positive constant satisfying $\kappa_3 \leq \min(\beta_i)$. Thus, Lyapunov derivative (51) satisfies condition (5). Meanwhile, Lyapunov function (48) also satisfies $\kappa_1 \|\mathbf{e}\|^2 \leq V = 0.5(\|\mathbf{e}\|^2 + \|\mathbf{s}\|^2) \leq \kappa_2 \|\mathbf{e}\|^2$ or equivalently $\kappa_1 \|\mathbf{e}\| \leq V \leq \kappa_2 \|\mathbf{e}\|$. Therefore, condition (4) holds for all $\kappa_1 \leq 0.5$ and $\kappa_2 \geq 0.5$. The application of Lemma 1 for system (47) and given the relationship between class kappa functions and positive-definite functions, together with Lemma 3, one can conclude that $\mathbf{e}(t)$ is terminally stable to the zero equilibrium, or \mathbf{q} approaches to \mathbf{q}_d within a finite time.

Remark 3: Integral actions of sliding manifolds (23) and (37) tend to mitigate chattering in system responses. In both schemes 1 and 2, the convergence of the outputs at phase 2 is achieved from the Mittag-Leffler stability.

5. Adaptive integral fractional-order fast terminal sliding mode with fault-tolerant control

Robustness of controllers (22) and (36) is based on the SMC methodology. However, their structures are fixed and may not be flexible enough to adapt with large uncertainties in the working environment while maintaining control performance. To remedy, we respectively propose two adaptive versions for robust controllers (22) and (36) as follows:

$$\hat{\mathbf{T}} = \mathbf{M}(\mathbf{q})\{\ddot{\mathbf{q}}_d - D_t^{2-\alpha}[\beta(\mathbf{e} + \mathbf{s}) + \lambda \mathbf{s}^{\zeta_1} + \mathbf{K} \text{sgn}(\mathbf{s})]\} + \mathbf{C}(\mathbf{q}, \dot{\mathbf{q}})\dot{\mathbf{q}} + \mathbf{G}(\mathbf{q}) - \hat{\mathbf{U}}(\mathbf{q}, \dot{\mathbf{q}}, \ddot{\mathbf{q}}, \hat{\mathbf{p}}, \hat{\mathbf{D}}, \phi) \tag{52}$$

with respect to manifold (23), and

$$\hat{\mathbf{T}} = \mathbf{M}(\mathbf{q})\{\ddot{\mathbf{q}}_d - D_t^{2-\alpha}[\beta \mathbf{e} + \gamma \mathbf{e}^{\zeta_2} + \beta \mathbf{s} + \mathbf{K} \text{sgn}(\mathbf{s})]\} + \mathbf{C}(\mathbf{q}, \dot{\mathbf{q}})\dot{\mathbf{q}} + \mathbf{G}(\mathbf{q}) - \hat{\mathbf{U}}(\mathbf{q}, \dot{\mathbf{q}}, \ddot{\mathbf{q}}, \hat{\mathbf{p}}, \hat{\mathbf{D}}, \phi) \tag{53}$$

for sliding surface (37). Therein, we provide an adaptation observer in the feedback loops for estimating concurrently uncertain robot parameters $\hat{\mathbf{p}}$, unknown disturbances $\hat{\mathbf{D}}$, and faults ϕ of motors by estimating the equivalent component $\hat{\mathbf{U}}(\mathbf{q}, \dot{\mathbf{q}}, \ddot{\mathbf{q}}, \hat{\mathbf{p}}, \hat{\mathbf{D}}, \phi)$ as described by

$$\begin{aligned} & s^T D_t^{\alpha-2} \mathbf{M}^{-1} \left[\mathbf{U}(\mathbf{q}, \dot{\mathbf{q}}, \ddot{\mathbf{q}}, \mathbf{p}, \mathbf{D}, \phi) - \hat{\mathbf{U}}(\mathbf{q}, \dot{\mathbf{q}}, \ddot{\mathbf{q}}, \hat{\mathbf{p}}, \hat{\mathbf{D}}, \phi) \right] \\ & = -[\mathbf{U}(\mathbf{q}, \dot{\mathbf{q}}, \ddot{\mathbf{q}}, \mathbf{p}, \mathbf{D}, \phi) - \hat{\mathbf{U}}(\mathbf{q}, \dot{\mathbf{q}}, \ddot{\mathbf{q}}, \hat{\mathbf{p}}, \hat{\mathbf{D}}, \phi)]^T \Upsilon [\mathbf{U}(\mathbf{q}, \dot{\mathbf{q}}, \ddot{\mathbf{q}}, \mathbf{p}, \mathbf{D}, \phi) - \hat{\mathbf{U}}(\mathbf{q}, \dot{\mathbf{q}}, \ddot{\mathbf{q}}, \hat{\mathbf{p}}, \hat{\mathbf{D}}, \phi)] \end{aligned} \tag{54}$$

where $\Upsilon = \text{diag}(\Upsilon_1, \dots, \Upsilon_{2n}) \in \mathbb{R}^{2n \times 2n}$ is a diagonal matrix of adaptation parameters. Notably, only one adaptive mechanism (54) is effectively utilized for two control laws (52) and (53). Such controllers achieve both robust and adaptive features, a fast and flexible manner. These advantages are incorporated in the following theorems.

Theorem 3: Control structure (52), where uncertainty equivalence $\hat{\mathbf{U}}(\mathbf{q}, \dot{\mathbf{q}}, \ddot{\mathbf{q}}, \hat{\mathbf{p}}, \hat{\mathbf{D}}, \phi)$ is estimated by fractional adaptation observer (54), asymptotically drives the robot outputs $\mathbf{q}(t)$ to destinations $\mathbf{q}_d(t)$.

Proof: We begin with a positive-definite Lyapunov candidate

$$V = 0.5(\mathbf{s}^T \mathbf{s} + \tilde{\mathbf{U}}^T \Upsilon \tilde{\mathbf{U}}) > 0, \tag{55}$$

where $\tilde{\mathbf{U}} = \mathbf{U} - \hat{\mathbf{U}}$ is estimation errors of uncertainties, faults, and disturbances. The time derivative of Lyapunov function (55) is written as

$$\dot{V} = \mathbf{s}^T \dot{\mathbf{s}} + \tilde{\mathbf{U}}^T \Upsilon \dot{\tilde{\mathbf{U}}}. \tag{56}$$

Respectively substituting manifold derivative (26) and robot model (21) into Eq. (56), one gets

$$\dot{V} = \mathbf{s}^T \{ D_t^{\alpha-2} [\mathbf{M}^{-1}(\mathbf{T} + \mathbf{U} - \mathbf{C}\dot{\mathbf{q}} - \mathbf{G}) - \ddot{\mathbf{q}}_d] + \boldsymbol{\beta}(\mathbf{q} - \mathbf{q}_d) \} + \tilde{\mathbf{U}}^T \Upsilon \dot{\tilde{\mathbf{U}}}. \tag{57}$$

Substitution of controller (52) and its adaptive estimator (54) into Eq. (57) leads to

$$\dot{V} = \mathbf{s}^T \left\{ \left[-\boldsymbol{\beta}(\mathbf{e} + \mathbf{s}) - \lambda \mathbf{s}^{\zeta_1} - \mathbf{K} \operatorname{sgn}(\mathbf{s}) + D_t^{\alpha-2} \mathbf{M}^{-1} \tilde{\mathbf{U}} \right] + \tilde{\mathbf{U}}^T \Upsilon \dot{\tilde{\mathbf{U}}} \right\} \tag{58}$$

which is simplified as

$$\dot{V} = -\mathbf{s}^T \boldsymbol{\beta} \mathbf{s} - \mathbf{s}^T \lambda \mathbf{s}^{\zeta_1} - \mathbf{s}^T \mathbf{K} \operatorname{sgn}(\mathbf{s}), \tag{59}$$

similarly to expression (29). Since the derivative (59) of the Lyapunov function (55) is negative definite, both \mathbf{s} and $\tilde{\mathbf{U}}(\mathbf{q}, \dot{\mathbf{q}}, \ddot{\mathbf{q}}, \tilde{\mathbf{p}}, \tilde{\boldsymbol{\phi}}, \tilde{\mathbf{D}})$ approach zero as time goes to infinity. Therefore, upon the convergence of manifold (23) to zeros, the stability of the outputs can be proven similarly as in the case of *Theorem 1*.

Theorem 4: Control structure (53) with fractional adaptation observer (54) for estimating total uncertainty $\tilde{\mathbf{U}}(\mathbf{q}, \dot{\mathbf{q}}, \ddot{\mathbf{q}}, \tilde{\mathbf{p}}, \tilde{\boldsymbol{\phi}}, \tilde{\mathbf{D}})$ asymptotically drives generalized coordinates $\mathbf{q}(t)$ of dynamics (17–18) to their destinations $\mathbf{q}_d(t)$.

Proof: We reconsider a positive Lyapunov candidate (55) with its derivative (56). Similar to proof of *Theorem 3*, we respectively substitute manifold derivative (40), robot dynamics (21) into Eq. (56), then we obtain

$$\dot{V} = \mathbf{s}^T \{ D_t^{\alpha-2} [\mathbf{M}^{-1}(\mathbf{T} + \mathbf{U} - \mathbf{C}\dot{\mathbf{q}} - \mathbf{G})] + \boldsymbol{\beta} \mathbf{e} + \boldsymbol{\gamma} \mathbf{e}^{\zeta_2} \} + \tilde{\mathbf{U}}^T \Upsilon \dot{\tilde{\mathbf{U}}}. \tag{60}$$

Inserting control scheme (53) and its adaptation mechanism (54) into expression (60) to get

$$\dot{V} = \mathbf{s}^T [-\boldsymbol{\beta} \mathbf{s} - \mathbf{K} \operatorname{sgn}(\mathbf{s}) + D_t^{\alpha-2} \mathbf{M}^{-1} \tilde{\mathbf{U}}] + \tilde{\mathbf{U}}^T \Upsilon \dot{\tilde{\mathbf{U}}}. \tag{61}$$

which is reduced as

$$\dot{V} = -\mathbf{s}^T \boldsymbol{\beta} \mathbf{s} - \mathbf{s}^T \mathbf{K} \operatorname{sgn}(\mathbf{s}). \tag{62}$$

The negative derivative (62) assures the convergence of both \mathbf{s} and $\tilde{\mathbf{U}}$. The next steps for proving stability can be conducted similarly to that of *Theorem 2*.

Remark 4: Switching action of controllers (52) and (53) with positive gains $\mathbf{K} = \operatorname{diag}(K_i)$ ($i = 1-2n$) is to keep the robustness of robot outputs. Too high gains \mathbf{K} cause much chattering at control inputs and robot responses. Otherwise, low gains \mathbf{K} cannot maintain the system robustness. Therefore, choosing upper boundary of \mathbf{K} should be considered to assure the consistency of robot outputs while preventing much chattering.

To summarize, the proposed adaptive robust control system for fault tolerance (AIFO-FTSMC) is presented as per the diagram shown in Fig. 2, wherein Block A denotes control laws (52) and (53), Block B indicates adaptation observer (54), and Block C characterizes for the robot dynamics (17–18). For teleoperation, Block D shows the path planning, which may be generated by using a joystick in the case of manual control. Thus, a human-inspired approach [24]-[23] may be integrated into this control system to serve the purpose.

6. Results and discussion

In this section, effectiveness of the proposed approach is verified by simulation, experiment, and comparison with other control techniques.

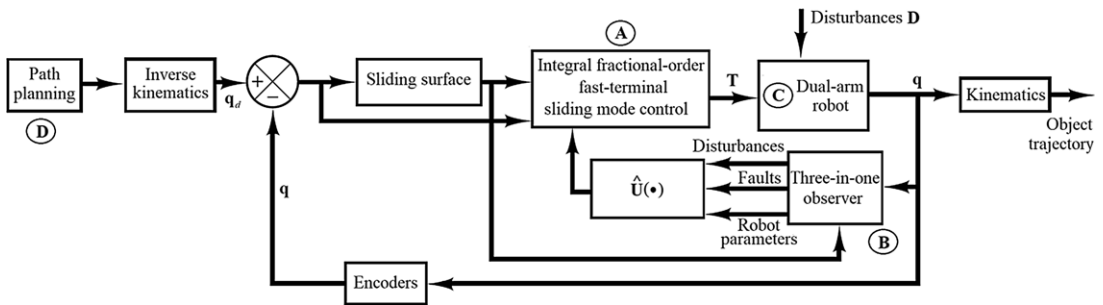


Figure 2. Control system diagram.

6.1. Simulation

We utilize a 4DOFs-DAR described in ref. [19] as a testbed to verify the control performance for two versions (52) and (53) coupled with observer (54) of our AIFO-FTSMC. In case of conventional robot dynamics [32], four nonlinear ordinary differential equations are converted into the form of eight state-space equations whereas (q, \dot{q}) are state variables. In this study, robot modeling is enhanced as a fractional-order state-space dynamics. Thus, a couple $(q, D_t^\eta q)$ is considered as state variables in simulation. The robot specifications are listed in Table II and control parameters are provided in Table III. For the sake of simulation, the faults of motors influencing on DAR are adopted from ref. [6] as $\phi(\dot{q}, q, T) = [\phi_1 \ 0 \ \phi_3 \ 0]^T$, whose components given by

$$\phi_1 = 10^3 (15 \sin q_1 q_2 + 2 \cos \dot{q}_1 q_2 + 8 \cos \dot{q}_1 \dot{q}_2) \text{ for } T_{f1} \geq 4, \tag{63}$$

$$\phi_3 = -0.8 T_3 \text{ for } T_{f1} \geq 4.5, \tag{64}$$

and $\eta = \text{diag}(1.5, 0, 1.2, 0)$. This implies that fault ϕ_1 appears at the 1st motor since the 4th sec, the 3rd motor reduces 80% efficiency after 4.5 s, while the 2nd and 4th motors have no fault.

The path $r_d(x, y, t)$ is generated similarly as per [32]. Accordingly, two grippers are controlled to move from points $(-80, 70)$ and $(80, 70)$ to the points $(-60, 150)$ and $(-50, 150)$, pick an object up, transfer it following a half-quarter of a circle of radius 55 mm to avoid an obstacle placed at center $(0, 150)$. Notably, the initial positions of grippers are given by conditions $q(0)$ and $\dot{q}(0)$ through the kinematic relation.

The DAR responses are presented respectively in Figs. 3, 4, 5 and 6. It is observed that various fractional-order (FO) values make a difference in transient states while the robot links rotate to desired angles asymptotically. Without any overshoot, responses of control law 2 with finite-time tracking of the outputs appear better than those of law 1. The overshoot occurs at the case $FO = 0.95$ of law 1 while no overshoot is observed at the other cases. The adaptation mechanism compensates well for faults of motors. Their impact on the outputs looks insignificant but when zooming in, the 1st motor’s fault causes a small deviation at motions of links 1 and 2 from the 4th s, and fault at the 3rd motor causes a slight divergence at rotations of links 3 and 4 from 4.5 s. Changing FO may influence the fault compensation. Despite the advantage from fault compensation, the impact, although negligible, is still observed in the tracking errors as shown in Figs. 7 and 8. Faults cause a small deformation of e_1 and e_2 at 4 s, e_3 and e_4 at 4.5 s. Generally, the steady-state tracking errors approach zeros owing to the integral action in the controller.

6.2. Experiments

A laboratory set up for the dual-arm robot is depicted in Fig. 9. Here, we used two Magician[®] manipulators as a dual-arm cooperative manipulation. Each manipulator has four DOFs. However, this work is concerned with only two DOFs but not the base rotation and end-effector motion. Four servo motors are

Table II. Robot parameters.

DAR

$m_1 = m_3 = 0.25$ kg; $m_2 = m_4 = 0.27$ kg; $l_1 = l_3 = 135$ mm; $l_2 = l_4 = 147$ mm;
 $I_1 = I_3 = 0.03$ kgm²; $I_2 = I_4 = 0.036$ kgm²; $k_1 = k_3 = 65$ mm;
 $k_2 = k_4 = 70$ mm; $m = 0.3$ kg; $\zeta = 0.35$; $d_1 = 10$ mm; $d_2 = 147$ mm;

Nonlinear frictions at joints

$b_1 = b_2 = b_3 = b_4 = 110$; $\mu_1 = \mu_2 = \mu_3 = \mu_4 = 0.4$; $\eta = \eta_1 = \eta_2 = \eta_3 = \eta_4 = 0.65$;

Initial conditions

$\dot{\mathbf{q}}(0) = \mathbf{0}_{1 \times 4}$; $\mathbf{q}(0) = [0 \quad 5\pi/6 \quad \pi \quad -5\pi/6]^T$;

Table III. AIFO-FTSMC gains.

Scheme 1	Scheme 2
$\beta = \text{diag}(5,4,4,3)$;	$\beta = \text{diag}(4,5,3.5,3)$;
$\lambda = \text{diag}(4,5,3,5) \times 10^{-2}$;	$\gamma = \text{diag}(1,2.5,2,3) \times 10^{-1}$;
$\mathbf{K} = \text{diag}(4,4,5,5)$;	$\mathbf{K} = \text{diag}(5,4,6,5)$;
$\zeta_1 = 0.8$; $\varepsilon = 0.05$;	$\zeta_2 = 3$; $\varepsilon = 0.05$;
$\Upsilon = \text{diag}(1.2,1.6,0.8,1.4)$;	$\Upsilon = \text{diag}(1.4,1.2,1.7,0.9)$;

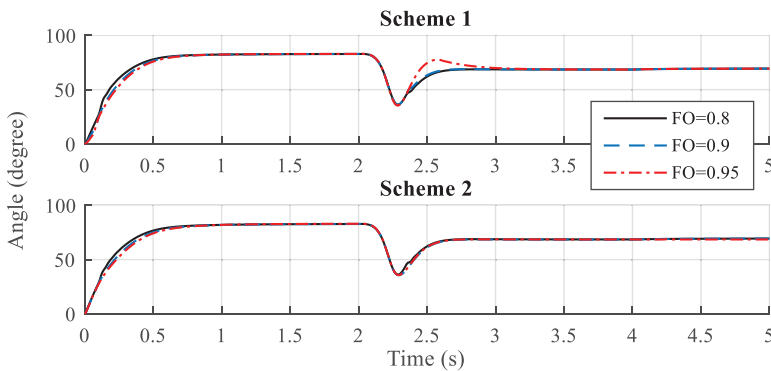


Figure 3. Simulation – link 1 rotation.

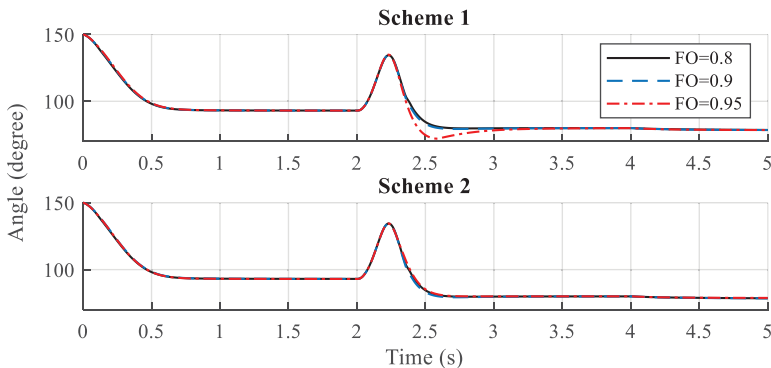


Figure 4. Simulation – link 2 rotation.

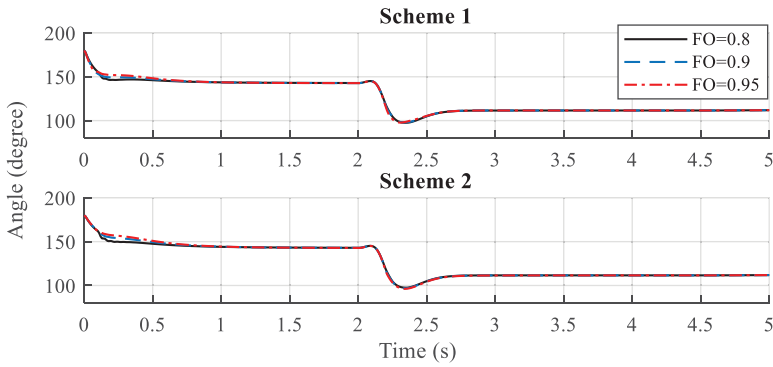


Figure 5. Simulation – link 3 rotation.

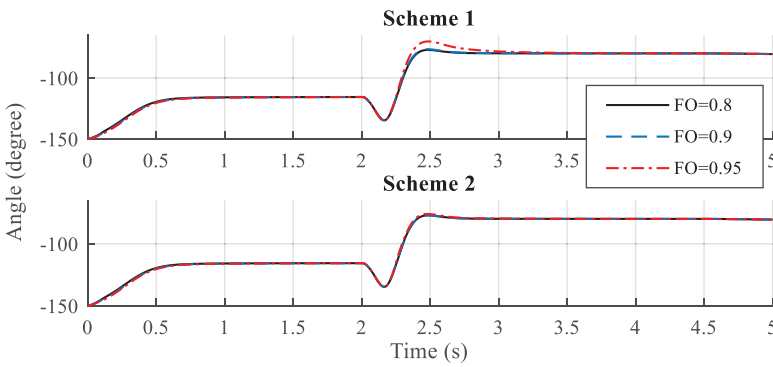


Figure 6. Simulation – link 4 rotation.

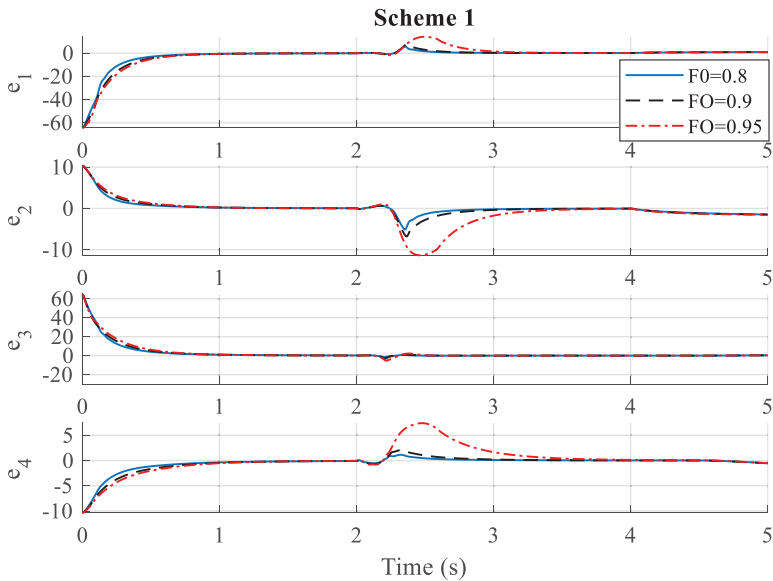


Figure 7. Simulation – tracking errors of scheme 1.

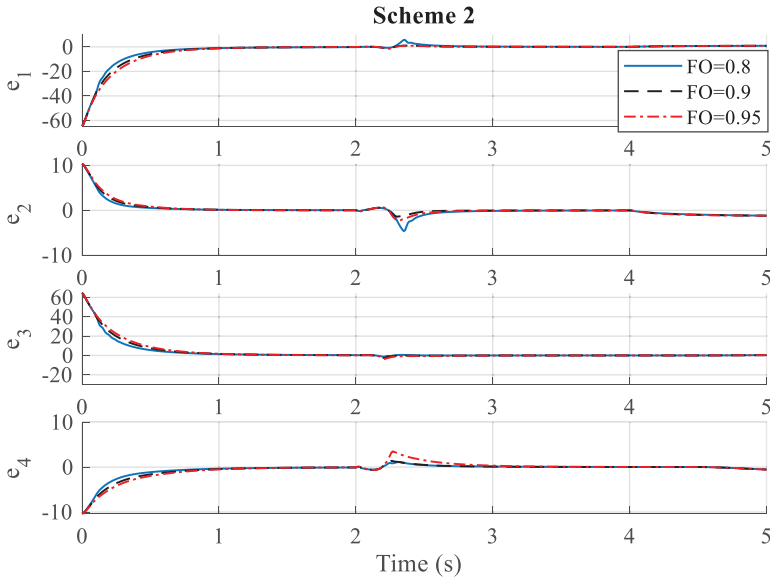


Figure 8. Simulation – tracking errors of scheme 2.

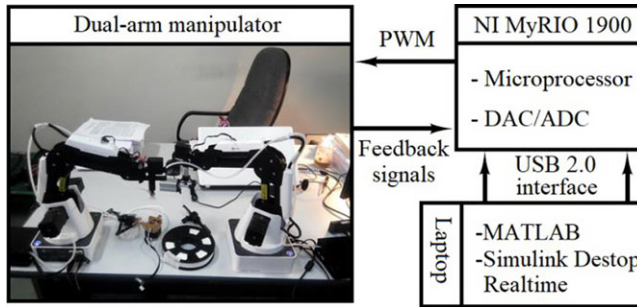


Figure 9. Diagram of experimental setup.

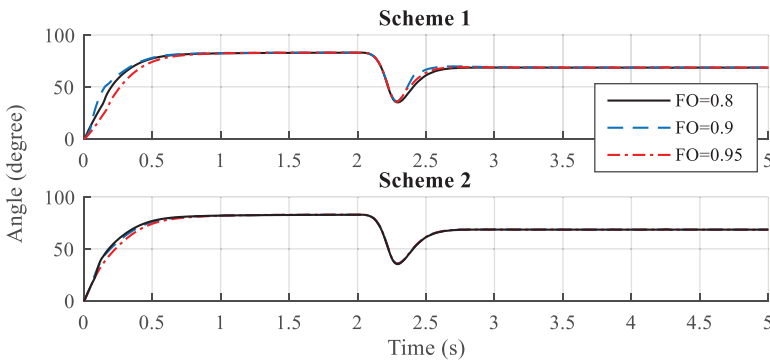


Figure 10. Experiment – link 1 rotation.

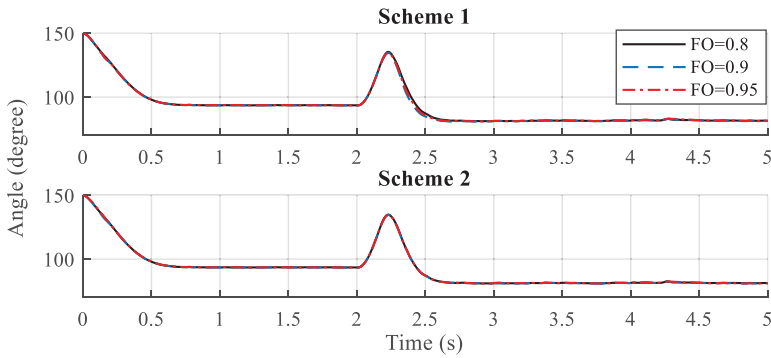


Figure 11. Experiment – link 2 rotation.

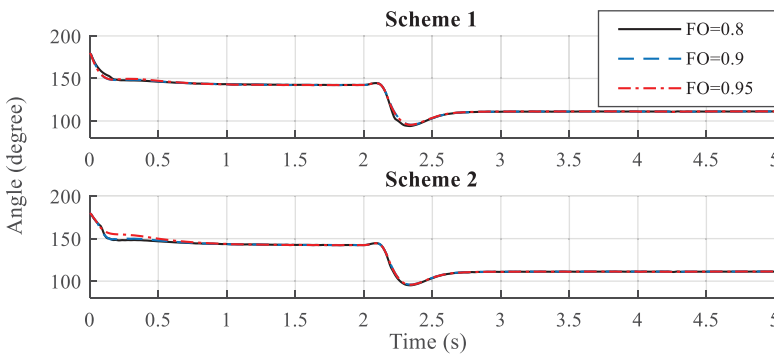


Figure 12. Experiment – link 3 rotation.

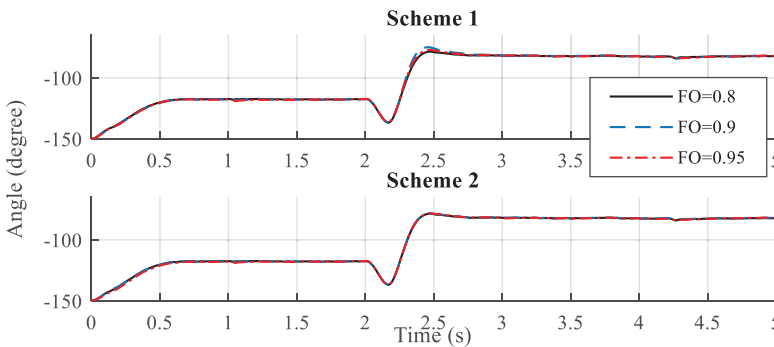


Figure 13. Experiment – link 4 rotation.

used for rotating joints with integrated encoders of 4096 resolution. For connecting the DAR for computer control, we use an embedded device, namely myRIO-1900. This device includes a Xilinx FPGA, a dual-core Cortex processor, and DAC/ADC module. Control algorithms are coded and compiled on MATLAB®/Simulink®. We use Desktop Real-Time™ that provides a real-time kernel for executing a Simulink-connected DAR model on a laptop. DAR runs real-time with PWM control signals while feeding joint rotations measured by encoders back to myRIO device.

Consistently with simulation, we run AIFO-FTSMC algorithms for three fractional orders $\alpha = 0.8$, 0.9, and 0.95. The experiment results are shown in Figs. 10, 11, 12, 13, 14, and 15. As clearly observed in Figs. 10, 12, and 13, scheme 2 displays better performance than scheme 1. Outputs of scheme 2 are

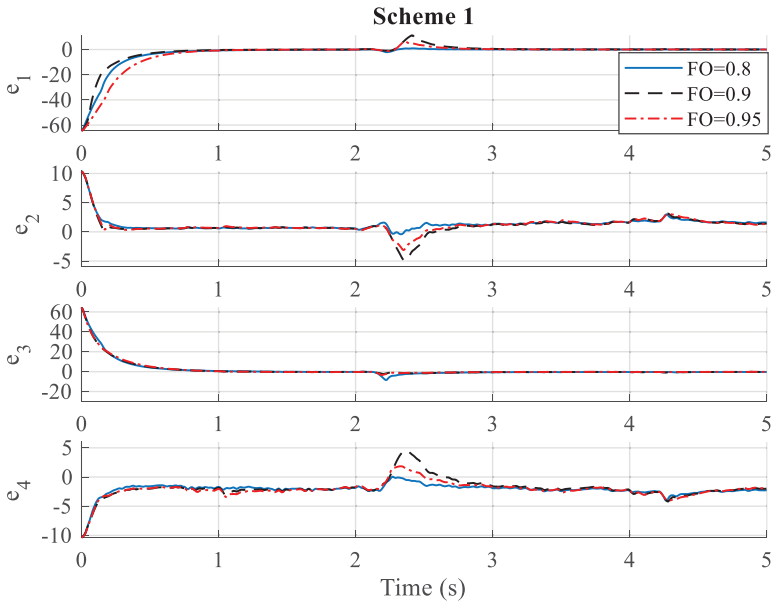


Figure 14. Experiment – tracking errors of scheme 1.

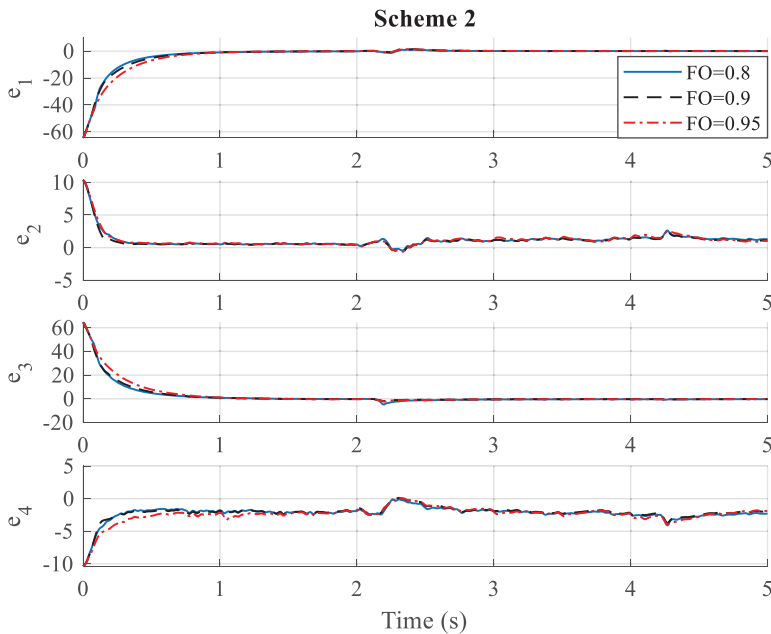


Figure 15. Experiment – tracking errors of scheme 2.

kept consistently when changing fractional orders. While simulation outputs are smooth, experimental ones exhibit some oscillations. Simulation responses reach destinations precisely while some negligible deviations are observed in experimental ones. Depicted in Figs. 14 and 15, the tracking errors, especially e_2 and e_4 , still display some little oscillations due to perturbances and noises induced by sensors and actuators, signal processing at ADC/DAC module, and faults. A low-pass filter is used for eliminating noises at feedback signals from encoders. The impact of noises on experimental outputs is thus reduced.

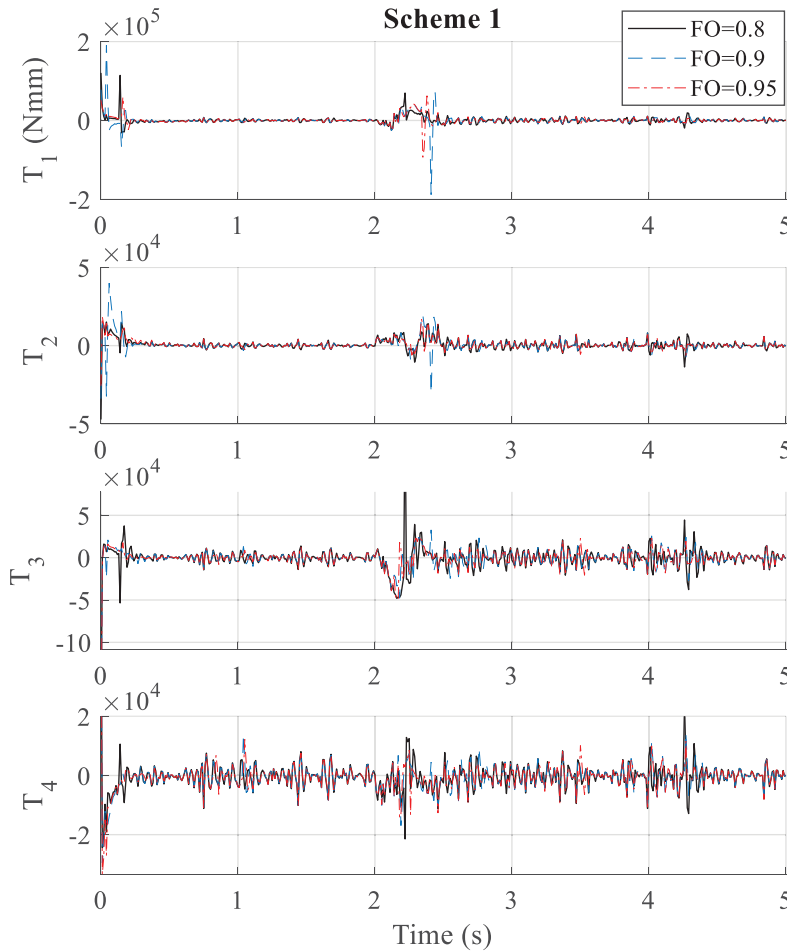


Figure 16. Experiment – control inputs of scheme 1.

The influence of faults in experimental outputs is not demonstrated on a new laboratory DAR in which no fault is detected.

Notably, experiment platform does not involve force sensors. Thus, control inputs at Figs. 16 and 17 are acquired from PWM block of Desktop Real-Time™ and processed via three others including PWM–speed and speed–torque blocks together with a low-pass filter. Control inputs that torque at robot joints show steady-state oscillations due to implementation issues of the practical control system and the signum function in the control structure.

Object trajectories $\mathbf{r}(x, y, t)$ depicted in Figs. 18 and 19 are obtained from rotations $\mathbf{q}(t)$ of links and robot kinematics. The robot completes its duty of picking up and moving objects to their destination precisely. The various cases exhibit a little bit of difference in followed paths, all reaching the same destinations.

Remarkably, the main objective of the adaptive approximator is not to estimate robot parameters, disturbances, and faults separately. This adaptive mechanism supports controller by finding proper values $\hat{\mathbf{U}}(\bullet)$ to converge the robot outputs following the desired trajectory. Figure 20 shows an illustrative result of three-in-one estimation by adaptive mechanism. Four components of estimated function $\tilde{\mathbf{U}}(\bullet)$ asymptotically reach zeros. This implies that estimated values $\hat{\mathbf{U}}(\bullet)$ approach to true values $\mathbf{U}(\bullet)$.

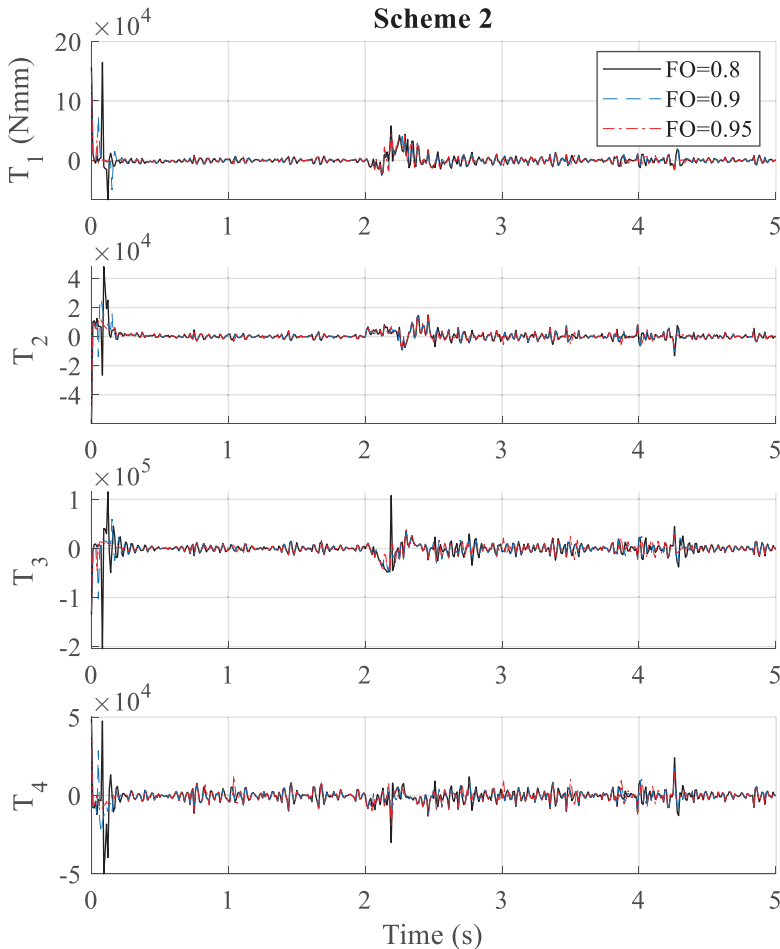


Figure 17. Experiment – control inputs of scheme 2.

6.3. Comparison

In the control of DARs, the techniques reported in refs. [20, 32] and our current study adopt the same SMC core while backstepping is used in ref. [22] to achieve robustness. The structure of AIFO-FTSMC appears to be more complex than that of the SMC core used in refs. [20, 32] as it can deal with more control objectives, faulty conditions, and incorporates components for fast terminal stability. In practical applications, using only backstepping would make it hard to maintain the output consistency, especially in face of disturbances.

For adaptive features of DARs, different approaches are developed in the works mentioned. In the development of the adaptive estimator, our study utilizes STC, while [32] relies on fuzzy logic, [20] uses neural networks and [22] combines neural networks with composite learning. Integrating such adaptive features is expected to make the robot operations more resilient and intelligent. Notably, control performance is verified by simulation only in ref. [32] while our study and [20] involve simulation and experimental verifications. The backstepping approach [22] needs recursive manipulation and may assure robustness against both structural and unstructured uncertainties if combined with SMC. The SMC cores use fixed first/second derivative orders, assuring asymptotic convergence [20, 22, 32] while our I-FTSMC involves variable orders of fractional derivatives and flexible control gains, making a quick finite-time convergence. This improves the adaptation of control system.

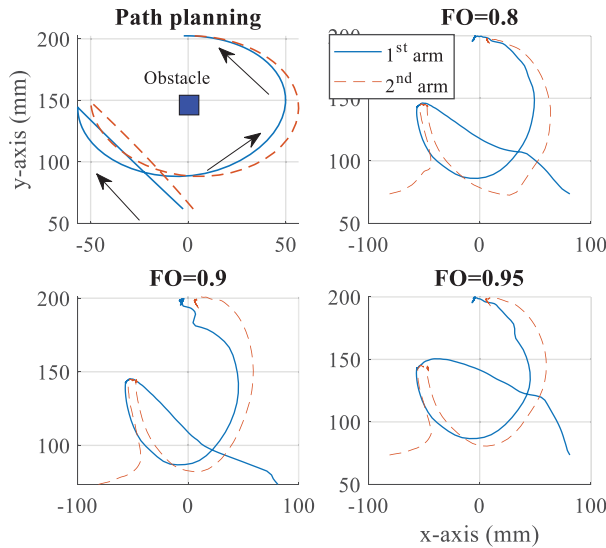


Figure 18. Experiment – object path of scheme 1.

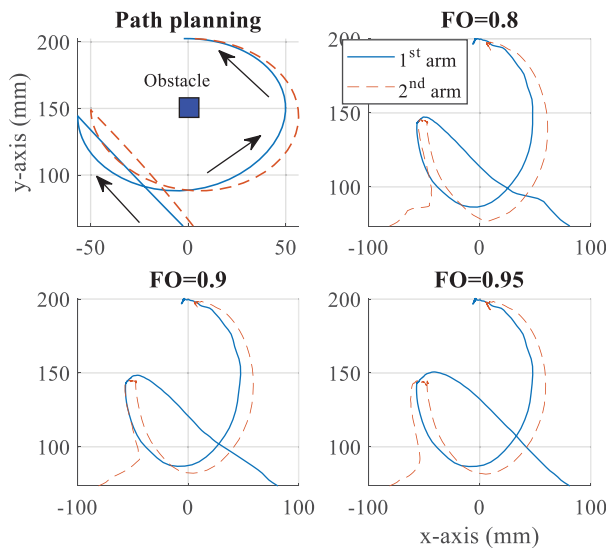


Figure 19. Experiment – object path of scheme 2.

Fuzzy adaptation in ref. [32] does not directly approximate uncertain parameters and disturbances. Rather, it adjusts control gains to adapt with uncertainties and disturbances. Neural adaptation proposed in ref. [20], addresses particularly on a certain type of nonlinearities, the output hysteresis. Here, in our STC adaptation, a three-in-one observer can concurrently estimate motors fault, parametric uncertainty, and disturbance. Indeed, fuzzy estimator [32] requires many intermediate steps (preprocessing, fuzzification, inference, defuzzification, and processing) and needs many local parameters. Since neural mechanisms [20, 22] use many weight gains in multi-inputs, multi-layers, and multi-outputs of the neural network, the resulting controllers represent complex structures and, hence, involve a computational burden with a certain time for estimation and identification. Our STC mechanism is simpler in structure and easy to implement with fewer gains, yet able to estimate simultaneously several targets. While the bimanual controller based on composite learning algorithm and online neural network [22] can display

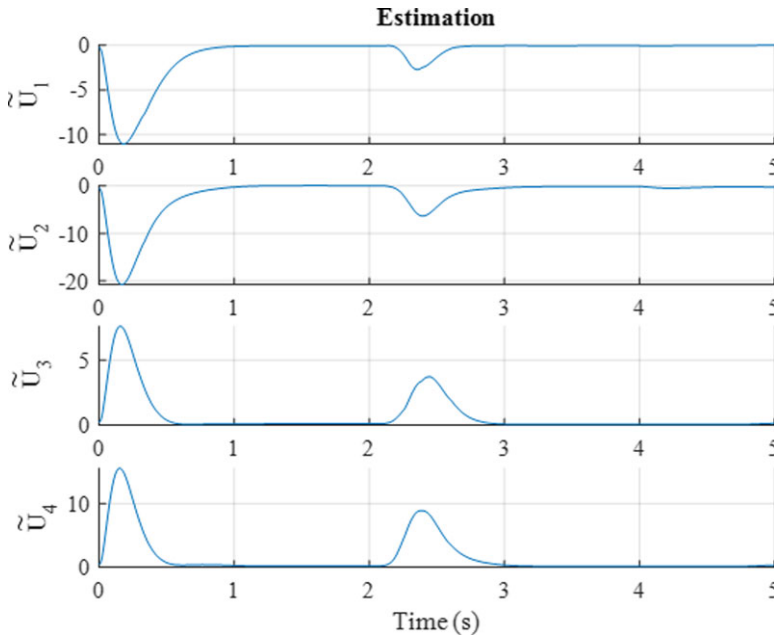


Figure 20. Approximating equivalent component $\hat{U}(\bullet)$ for scheme 2 and $FO = 0.95$.

two important features of DARs, namely, mimic human behavior and learning ability, along with refs. [20] and [32], do not consider the impact of motor failures. On the contrary, our AIFO-FTSMC can operate in harsh conditions with the occurrence of motor faults.

In summary, key features of the mentioned control approaches are presented in Table IV. The performance comparison together with simulation and experimental results shown above have confirmed the merits of our proposed AIFO-FTSMC schemes.

For comparing the quantitative achievements of various control approaches, Table V shows specifications of robot outputs including maximum overshoot, settling time, and steady-state error for each control method. It seems that with the same methodology, for a control system being more complex with many functions, its quality is not better than control systems having fewer functions.

7. Conclusion

This paper has presented a fault-tolerant tracking control system for dual-arm robots using adaptive fractional-order integral fast terminal sliding mode. By combining prominent features of the integral, fast terminal sliding mode, fault-tolerant control, and self-tuning control with fractional-order systems, we have designed new controllers for dual-arm robots to achieve both robustness and adaptive capability. As shown qualitatively and quantitatively, advantages of the proposed control system include reaching the desired inputs and maintaining the tracking performance, mitigating chattering, while achieving rapid and terminal convergence without knowledge of actuator faults, uncertain parameters, and unknown disturbances. The adaptive behavior can be attributed to a three-in-one observer with a reduced estimation time as only one equivalent term needs to be estimated instead of three separate components. With the support from the adaptive observer, the control system exhibits superior performance with self-adjusting ability to immunize large uncertainties. Such proposed control framework along with its merits constitute the new contributions of this paper. Extensive simulations and experiments confirm the advantages of our control approach in comparison with other advanced control techniques available. Our future

Table IV. Features of various control systems.

Approach	AIFO-FTSMC	Fuzzy SMC [32]	Neural SMC [20]	Machine learning [22]
Core	FO-I-FTSMC	SMC	SMC	Backstepping
Features	Adjustable derivative orders. Multi-goal estimation. Rapid and finite-time convergence.	Fixed derivative orders. Single estimation. Infinite convergence.	Fixed derivative orders. Single estimation. Infinite convergence.	Fixed derivative orders. Multi-goal estimation. Infinite convergence.
Adaptive technique	STC.	Fuzzy logic.	Neural networks.	Composite learning. Neural networks.
Estimation ability	Faults, uncertain parameters, and	Controller gains.	Output hysteresis.	Modelling uncertainty.

Table V. Characteristics of robot responses among various control approaches.

Approaches	AIFO-FTSMC (FO = 0.95)				Fuzzy SMC [32]				Neural SMC [20]				MRAC-SMC [19]				
	q ₁	q ₂	q ₃	q ₄	q ₁	q ₂	q ₃	q ₄	q ₁	q ₂	q ₃	q ₄	q ₁	q ₂	q ₃	q ₄	
Rotation of links																	
First phase																	
Settling time(s)	0.97	0.89	1.09	0.94	1.2	1.1	0.95	1.05	1.9	1.8	1.4	1.9	2.1	2	1.7	2	
Overshoot(°)	0	0	0	0	X	X	X	X	0	0	0	0	0	0	0	0	
Steady error(°)	1.8	2.04	1.6	2.7	X	X	X	X	0.84	0.3	1.7	0.3	0.4	0.2	0.2	0.6	
Second phase																	
Settling time(s)	1.04	0.95	0.43	1.1	0.9	1.1	1.05	1.05	1.4	1.4	1.1	1.6	1.7	1.4	1.6	1.8	
Overshoot(°)	7	7	12	6	X	X	X	X	0	0	0	0	0	0	0	0	
Steady error(°)	1.28	2.78	1.6	1.9	X	X	X	X	1.02	0.5	0.1	0.9	0.8	0.6	0.5	0.2	

“X” indicates that this value cannot be measured exactly on figures representing robot responses in ref. [32].

work will aim at incorporating learning schemes into the control structure and optimizing the fractional orders and control gains in order to further improve DAR’s performance.

Acknowledgments. L.A. Tuan is supported by Vietnam Maritime University.

Author contributions. L.A. Tuan and Q.P. Ha contributed to the study’s conception and design. L.A. Tuan performed data collection and analysis, did simulation and experiment, and wrote the manuscript. Q.P. Ha supervised this work. All authors read and approved the final manuscript.

Competing interests. The authors declare none.

Code or data availability. No.

Ethical standards. The authors assert that all procedures contributing to this work comply with the ethical standards of the relevant national and institutional committees on human experimentation and with the Helsinki Declaration of 1975, as revised in 2008.

References

- [1] M. Abbas and S. Dwivedy, "Adaptive control for networked uncertain cooperative dual-arm manipulators: An event-triggered approach," *Robotica* **40**(6), 1951–1978 (2022).
- [2] H. Hu, J. Cao and Y. Cao, "Prescribed time tracking control without velocity measurement for dual-arm robots," *Inf. Sci.* **629**, 533–550 (2023).
- [3] N. Lv, J. Liu and Y. Jia, "Dynamic modeling and control of deformable linear objects for single-arm and dual-arm robot manipulations," *IEEE Trans. Robot.* **38**(4), 2341–2353 (2022).
- [4] M. H. Korayem, A. M. Shafei and E. Sidei, "Symbolic derivation of governing equations for dual-arm mobile manipulators used in fruit-picking and the pruning of tall trees," *Comput. Electron. Agric.* **105**, 95–102 (2014).
- [5] P. Ghaf-Ghanbari, M. Mazare and M. Taghizadeh, "Active fault-tolerant control of a schonnflies parallel manipulator based on time delay estimation," *Robotica* **39**(8), 1518–1535 (2021).
- [6] M. Van and S. S. Ge, "Adaptive fuzzy integral sliding mode control for robust fault tolerant control of robot manipulators with disturbance observer," *IEEE Trans. Fuzzy Syst.* **29**(5), 1284–1296 (2021).
- [7] A. H. Korayem, S. R. Nekoo and M. H. Korayem, "Sliding mode control design based on the state-dependent Riccati equation: Theoretical and experimental robotic implementation," *Int. J. Control* **92**(9), 2136–2149 (2019).
- [8] W. Yan, Y. Liu, Q. Lan, T. Zhang and H. Tu, "Trajectory planning and low-chattering fixed-time nonsingular terminal sliding mode control for a dual-arm free-floating space robot," *Robotica* **40**(3), 625–645 (2022).
- [9] M. Van, X. P. Do and M. Mavrouniotis, "Self-tuning fuzzy PID-nonsingular fast terminal sliding mode control for robust fault tolerant control of robot manipulators," *ISA Trans.* **96**, 60–68 (2020).
- [10] A. M. Singh and Q. P. Ha, "Fast terminal sliding control application for second-order underactuated systems," *Int. J. Control Autom. Syst.* **17**(8), 1884–1898 (2019).
- [11] Q. Qin and G. Gao, "Screw dynamic modeling and novel composite error-based second-order sliding mode dynamic control for a bilaterally symmetrical hybrid robot," *Robotica* **39**(7), 1264–1280 (2021).
- [12] H. Dong, X. Yang and M. V. Basin, "Practical tracking of permanent magnet linear motor via logarithmic sliding mode control," *IEEE/ASME Trans. Mechatron.* **27**(5), 4112–4121 (2022).
- [13] X. Fu, H. Ai and L. Chen, "Integrated sliding mode control with input restriction, output feedback and repetitive learning for space robot with flexible-base, flexible-link and flexible-joint," *Robotica* **41**(1), 370–391 (2023).
- [14] F. Li, Z. Zhang, Y. Wu, Y. Chen, K. Liu and J. Yao, "Improved fuzzy sliding mode control in flexible manipulator actuated by PMAs," *Robotica* **40**(8), 2683–2696 (2022).
- [15] L. Xie, X. Yu and L. Chen, "Robust fuzzy sliding mode control and vibration suppression of free-floating flexible-link and flexible-joints space manipulator with external interference and uncertain parameter," *Robotica* **40**(4), 997–1019 (2022).
- [16] Y. Wang, L. Gu, Y. Xu and X. Cao, "Practical tracking control of robot manipulators with continuous fractional-order nonsingular terminal sliding mode," *IEEE Trans. Ind. Electron.* **63**(10), 6194–6204 (2016).
- [17] W. Jie, Z. Yudong, B. Yulong, H. H. Kim and M. C. Lee, "Trajectory tracking control using fractional-order terminal sliding mode control with sliding perturbation observer for a 7-DOF robot manipulator," *IEEE/ASME Trans. Mechatron.* **25**(4), 1886–1893 (2020).
- [18] X. Yu, J. Guo and J. Zhang, "Time delay estimation-based reactionless augmented adaptive sliding mode control of a space manipulator's pregrasping a target," *Robotica* **40**(9), 3136–3156 (2022).
- [19] L. A. Tuan, Y. H. Joo, P. X. Duong and L. Q. Tien, "Parameter estimator integrated-sliding mode control of dual arm robots," *Int. J. Control Autom. Syst.* **15**(6), 2754–2763 (2017).
- [20] Z. Liu, C. Chen, Y. Zhang and C. L. P. Chen, "Adaptive neural control for dual-arm coordination of humanoid robot with unknown nonlinearities in output mechanism," *IEEE Trans. Cybern.* **45**(3), 521–532 (2015).
- [21] L. A. Tuan, Y. H. Joo, L. Q. Tien and P. X. Duong, "Adaptive neural network second-order sliding mode control of dual arm robots," *Int. J. Control Autom. Syst.* **15**(6), 2283–2298 (2017).
- [22] Y. Jiang, Y. Wang, Z. Miao, J. Na, Z. Zhao and C. Yang, "Composite-learning-based adaptive neural control for dual-arm robots with relative motion," *IEEE Trans. Neural Netw. Learn. Syst.* **33**(3), 1010–1021 (2022).
- [23] Z. Li, W. Yuan, S. Zhao, Z. Yu, Y. Kang and C. L. P. Chen, "Brain-actuated control of dual-arm robot manipulation with relative motion," *IEEE Trans. Cogn. Devel. Syst.* **11**(1), 51–62 (2019).
- [24] B. Huang, Z. Li, X. Wu, A. Ajoudani, A. Bicchi and J. Liu, "Coordination control of a dual-arm exoskeleton robot using human impedance transfer skills," *IEEE Trans. Syst., Man, Cybern., Syst.* **49**(5), 954–963 (2019).
- [25] Z. Li, C. Xu, Q. Wei, C. Shi and C.-Y. Su, "Human-inspired control of dual-arm exoskeleton robots with force and impedance adaptation," *IEEE Trans. Syst., Man, Cybern., Syst.* **50**(12), 5296–5305 (2020).
- [26] A. Kochubei and Y. Luchko, *Handbook of Fractional Calculus with Applications* (De Gruyter, Berlin, Germany, 2019).
- [27] M. Raoufi and H. Delavari, "Experimental implementation of a novel model-free adaptive fractional-order sliding mode controller for a flexible-link manipulator, int," *J. Adapt. Control. Signal. Process.* **35**(10), 1990–2006 (2021).
- [28] H. Delavari and R. Jokar, "Intelligent fractional-order active fault-tolerant sliding mode controller for a knee joint orthosis," *J. Intell. Robot. Syst.* **102**(39) (2021).
- [29] Z. Ma, Z. Liu, P. Huang and Z. Kuang, "Adaptive fractional-order sliding mode control for admittance-based telerobotic system with optimized order and force estimation," *IEEE Trans. Ind. Electron.* **69**(5), 5165–5174 (2022).
- [30] P. V. Trieu, H. M. Cuong, H. Q. Dong, N. H. Tuan and L. A. Tuan, "Adaptive fractional-order fast terminal sliding mode with fault-tolerant control for underactuated mechanical systems: Application to tower cranes," *Autom. Constr.* **123**, 103533 (2021).
- [31] C. Yang, Y. Jiang, J. Na, Z. Li, L. Cheng and C. Su, "Finite-time convergence adaptive fuzzy control for dual-arm robot with unknown kinematics and dynamics," *IEEE Trans. Fuzzy Syst.* **27**(3), 574–588 (2019).

- [32] Y. Hacioglu, Y. Z. Arslan and N. Yagiz, “MIMO fuzzy sliding mode controlled dual arm robot in load transportation,” *J. Frankl. Inst.-Eng. Appl. Math.* **348**(8), 1886–1902 (2011).
- [33] Y. Li, Y. Q. Chen and I. Podlubny, “Stability of fractional-order nonlinear dynamic systems: Lyapunov direct method and generalized Mittag-Leffler stability,” *Comput. Math. Appl.* **59**(5), 1810–1821 (2010).
- [34] H. K. Khalil, *Nonlinear Systems* (3rd edn.) (Pearson, 2002).
- [35] M. A. D. Mermoud, N. Aguila-Camacho, J. A. Gallegos and R. Castro-Linares, “Using general quadratic Lyapunov functions to prove Lyapunov uniform stability for fractional order systems,” *Commun. Nonlinear Sci. Numer. Simul.* **22**(1), 650–659 (2015).
- [36] N. A.-Camacho, M. A. D. Mermoud and J. A. Gallegos, “Lyapunov functions for fractional order systems, commun,” *Nonlinear Sci. Numer. Simul.* **19**(9), 2951–2957 (2014).
- [37] S. Yu, X. Yu, B. Shirinzadeh and Z. Man, “Continuous finite time control for robotic manipulators with terminal sliding mode,” *Automatica* **41**(11), 1957–1964 (2005).